Hindawi
BioMed Research International
Volume 2022, Article ID 2276102, 9 pages
https://doi.org/10.1155/2022/2276102

Research Article

Improved Performance of Compartments in Detecting the Activity of Axial Spondyloarthritis Based on IVIM DWI with Optimized Threshold *b* Value

Qiang Ye, Zhuoyao Xie, Chang Guo, Xing Lu, Kai Zheng, and Yinghua Zhao

Department of Radiology, The Third Affiliated Hospital of Southern Medical University (Academy of Orthopedics, Guangdong Province), Guangzhou, Guangdong 510630, China

Correspondence should be addressed to Yinghua Zhao; zyh7258957@163.com

Received 16 October 2021; Revised 12 December 2021; Accepted 18 December 2021; Published 10 January 2022

Academic Editor: Ernesto Roldan-Valadez

Purpose. To explore the diagnostic performance of the optimized threshold *b* values on IVIM to detect the activity in axial spondyloarthritis (axSpA) patients. *Method*. 40 axSpA patients in the active group, 144 axSpA patients in the inactive group, and 20 healthy volunteers were used to evaluate the tissue diffusion coefficient (D_{slow}), perfusion fraction (f), and pseudodiffusion coefficient (D_{fast}) with *b* thresholds of 10, 20, and 30 s/mm^2. The Kruskal-Wallis test and one way ANOVA test was used to compare the different activity among the three groups in axSpA patients, and receiver operating characteristic (ROC) curve analysis was applied to evaluate the performance for D_{slow}, f, and D_{fast} to detect the activity in axSpA patients, respectively. *Results*. D_{slow} demonstrated a statistical difference between two groups ($P < 0.05$) with all threshold *b* values. With the threshold b value of 30 s/mm^2, f could discriminate the active from control groups ($P < 0.05$). D_{slow} had similar performance between the active and the inactive groups with threshold *b* values of 10, 20, and 30 s/mm^2 (AUC: 0.877, 0.882, and 0.881, respectively, all $P < 0.017$). Using the optimized threshold *b* value of 30 s/mm^2, f showed the best performance to separate the active from the inactive and the control groups with AUC of 0.613 and 0.738 (both $P < 0.017$) among all threshold *b* values. *Conclusion*. D_{slow} and f exhibited increased diagnostic performance using the optimized threshold *b* value of 30 s/mm^2 compared with 10 and 20 s/mm^2, whereas D_{fast} did not.

1. Introduction

Axial spondyloarthritis (axSpA) is a chronic inflammatory disease involving predominantly the sacroiliac joints (SIJ), the axial skeleton, and entheses [1], ultimately leading to significant disability and loss of social function [2]. According to data from multiple countries, the incidence of axSpA is 0.4-14 per 100,000 person-years [3]. However, no available agents have demonstrated a disease-modifying effect in axSpA [4]. Hence, an increasing number of treatment trials in axSpA are being conducted, heralding the potential availability of more effective treatments in the future. To make it possible for the comparison between trials of different agents, a noninvasive and quantitative method for evaluating the disease activity of patients with axSpA is highly desirable.

Magnetic resonance imaging (MRI) is an imaging modality of choice for assessing disease activity in axSpA [5]. Furthermore, disease activity in axial spondyloarthritis (axSpA) has been longitudinally associated with SIJ inflammation on MRI [6]. Le Bihan et al. [7] reported that the intravoxel incoherent motion (IVIM) diffusion-weighted imaging (DWI), respectively, measured the pure diffusion coefficient (D_{slow}), perfusion-related incoherent microcirculation coefficient (D_{fast}), and perfusion fraction (f). The diffusion of molecules is restricted in sacroiliitis since increased protein-rich fluids and inflammatory cells accumulate within the lesion in axSpA. The perfusion is also known to be raised because of the higher amount of blood or serum of capillary transported to the marrow cavity within the lesion in axSpA [8]. So, IVIM DWI was mainly proposed

to functionally and qualitatively diagnose the activity of axSpA [9]. But there has been much controversy surrounding the roles of D_{fast} and f for separating the active from nonactive patients with axSpA [10–12].

In previous studies, quantitative metrics of IVIM were turned out to be not very accurate, partially due to the limited sampling, low signal-to-noise ratio (SNR) for fast data acquisition, diffusion gradient polarity, and so on [13, 14]. First of all, some studies confirmed that segmented-unconstrained analysis should be preferred in the cases of a limited number of b values and finite SNRs. Tissue parameters derived from IVIM analysis depend on the threshold b value. With the analysis of data sampled from healthy individuals, the optimal threshold b value for liver IVIM analysis has been reported [15]. It had been demonstrated that the optimal threshold b value of 60 s/mm^2 could potentially provide better detection for liver fibrosis than threshold b values of 40, 80, 100, 150, and 200 s/mm^2 [16]. However, the optimal threshold b value for sacroiliitis IVIM analysis is still unclear. Therefore, in the current study, we explored how the selection of threshold b value impacts f, D_{slow}, and D_{fast} values and how threshold b value impacts IVIM technique's performance to detect the activity of axSpA patients.

2. Materials and Methods

2.1. Study Population. This prospective study was approved by our Institute Ethics Committee, and written informed consent was obtained from all participants (IRB number AN16327-001). According to the Assessment of Spondyloarthritis International Society criteria for axSpA [17], all patients diagnosed with axSpA were enrolled during the period from August 2017 to August 2019. The patients underwent erythrocyte sedimentation rate (ESR), C-reactive protein (CRP), and Spondyloarthritis Disease Activity Score (ASDAS). Within a week after the laboratory tests and clinical assessments, an MRI examination of the sacroiliac joints was performed using 3.0 T scanner. The exclusion criteria were defined as follows: (1) participants with contraindications cannot be scanned by MRI scanner; (2) patients with axial axSpA had peripheral joint involvement, such as hip, shoulder, and knee joints; (3) patients without IVIM DWI examination; and (4) MR images with low signal-to-noise ratio (SNR). Based on ASDAS and CRP [18], all patients with AS were classified as the active and inactive groups according to the following: the active group, ASDAS-CRP $\geq$ 1.3, and the inactive group, ASDAS-CRP $<$ 1.3 [19]. Meanwhile, 20 male healthy volunteers (16 males, 4 females; mean age 26.20 $\pm$ 5.71 years, range 21-47 years; mean weight 72.85 $\pm$ 20.40 kg, range 48–130 kg; mean height 173.8 $\pm$ 7.15 cm, range 168–190 cm) were enrolled as the control group. The volunteers were included with the criteria: (1) without a history of low back pain or trauma and (2) without a metallic foreign body.

2.2. MR Imaging Techniques. A 3.0Tesla Achieva MR imaging system (Philips Healthcare, Best, Netherlands) equipped with 32 channels body phased array coil was performed to enable the acquisition of high-resolution medical images. In this section, five standard MRI sequences were obtained: (a) Dixon fat-water separation coronal TSE T1WI (TSE T1WI mDixon), (b) Dixon fat-water separation coronal TSE T2WI (TSE T2WI mDixon), (c) axial T1-weighted turbine spin echo (T1-TSE), (d) axial T2-weighted spectral attenuated inversion recovery (T2W-SPAIR), and (e) axial IVIM DWI (Table 1). IVIM DWI was based on a single-shot DW spin-echo echo-planar imaging (EPI) with scanning time of 182 seconds.

2.3. Image Postprocessing and Measurement Analysis. A professional image postprocessing workstation with high computing power (PRIDE DWI Tool, IDL Virtual Machine Version 6.3, Philips Healthcare, Japan) was used to calculate complex image algorithm problems. The MRI medical images were imputed to the image postprocessing workstation for further processing.

Two radiologists with 10 and 3 years of experience in musculoskeletal MRI interpretation were involved for the recognition of lesions and delineation of ROIs independently, and then all parameters were acquired from IVIM DWI. Patients' clinical information were blinded to either radiologist. Intra- and interobserver agreement for 40 random patients (20 in the active group and 20 in the inactive group) were evaluated using the intraclass correlation coefficient (ICC) by the two radiologists. ICCs $\geq$ 0.75 were considered to be excellent and used for further analysis. The radiologist with 10 years of experience was responsible for measuring the remaining IVIM DW image data.

For the axSpA patients with visible bone marrow edema (BME) in SIJs on conventional MR images, only one free-hand region of interest (ROI) was drawn in the largest lesion of sacroiliitis on the axial map. If the area of BME was not large enough to draw an ROI, those patients will be included in the Non-BME group. For the Non-BME group, ROIs were placed in the subchondral lesions in the sacrum or the ilium. To reduce the impact of ROI on our results, the size of each ROI was chosen to be as large as possible with the exclusion of the blood vessels, adjacent bone cortex, cystic areas, necrosis, and fat metaplasia. For the healthy volunteers, ROIs were placed in the subchondral marrow in the middle areas of the sacrum or the ilium along the SIJs. The mean area of ROI was 24.08 mm^2 (range 18.5-36.7 mm^2). And then, the same ROIs were automatically replicated and pasted on the corresponding area on the D_{fast} and f maps at the same level. At last, the same ROI masks were propagated to all the other b values images (Figure 1).

According to the IVIM DWI theory proposed by Le Bihan et al. [7], DWI based on multiple b values is implemented in a biexponential model as

$$\frac{S_b}{S_0} = (1 - f)\exp(-b\,Dslow) + f\exp(-b\,Dfast), \quad (1)$$

where S_b represented the signal intensity of the pixel when the diffusion gradient is on and S_0 represents the signal intensity of the pixel when the diffusion gradient is off [20]. D_{slow} was obtained by a simplified linear fitting equation with b values higher than 200 s/mm^2 as Equation (2) [21]:

Table 1: Summary of MRI scan parameters.

Sequences	TSE T1WI mDixon	TSE T2WI mDixon	T1-TSE	T2W-SPAIR	IVIM DWI
Plane	Coronal	Coronal	Axial	Axial	Axial
TR/TE (ms)	569/20	2300/85	500/10	5200/70	4000/63.5
Thickness (mm)	3	3	6	5	4
Field of view (mm)	230 × 332	230 × 319	332 × 353	300 × 400	300 × 360
Intersection gap (mm)	0.5	0.5	1	0.5	1
SENSE factor	2.6	2	1.8	2.3	2.8
Matrix	272 × 325	288 × 394	272 × 343	236 × 406	100 × 120
Number of signal average (NSA)	1	1.5	1	1.2	2

IVIM DWI was based on b values = 0, 10, 20, 30, 50, 600, and 800 s/mm^2.

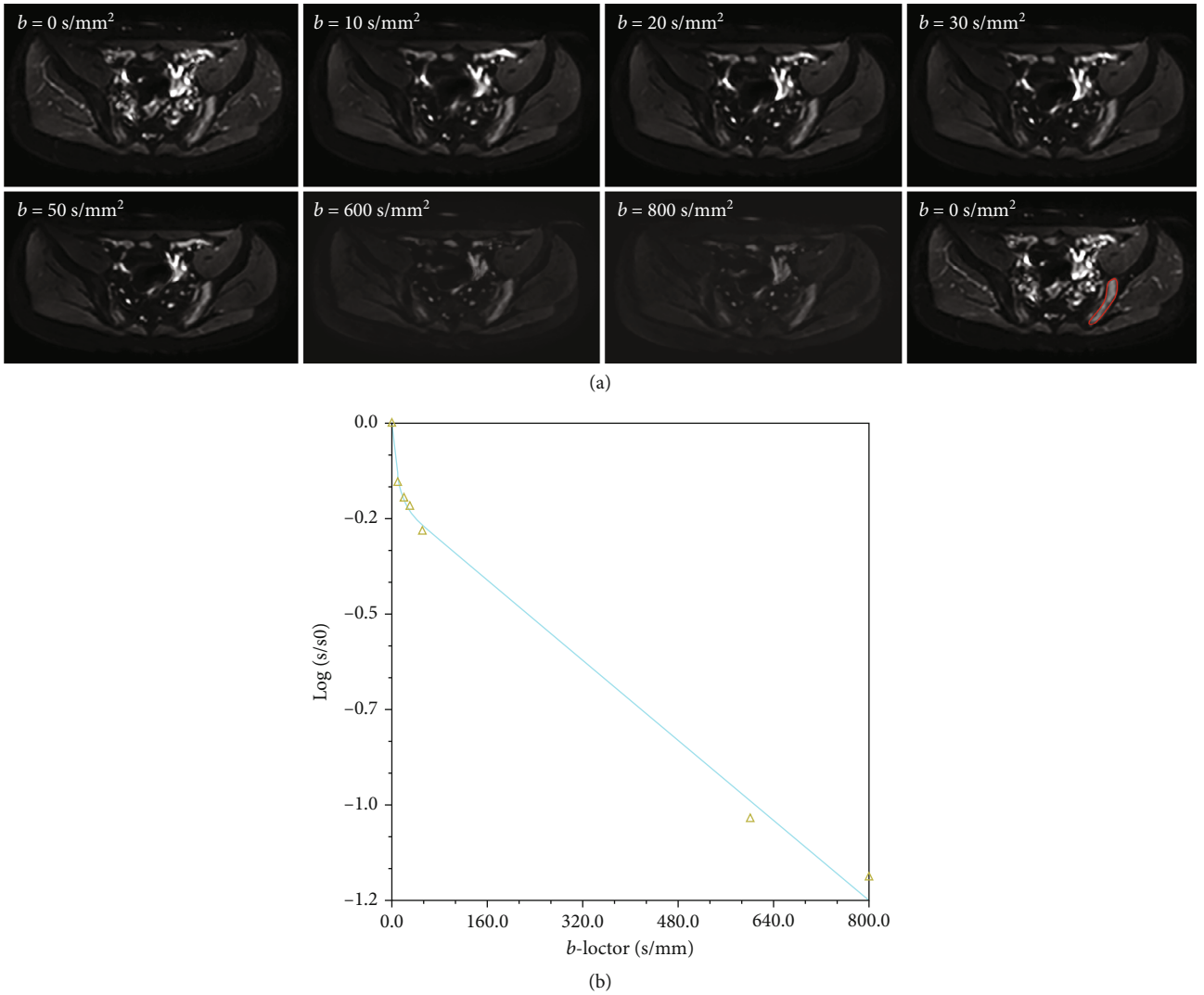

Figure 1: (a) Demonstration of diffusion-weighted images with 7 b values from a patient with axial spondyloarthritis (axSpA) and a region of interest (ROI) drawn in the lesion area on DWI of $b = 0$ s/mm^2. (b) The relationship between signals and b values for the lesion in the sacroiliac joint.

$$R^2 = \frac{1\text{-SSE}}{SS_{total}} \quad (2)$$

was applied to assess the consistency of fit, where SSE indicates the error sum of squares between the fitted curve and data and SS_{total} is defined as the total sum of squares between all the calculated values and their overall average.

To acquire high diagnostic performance, a threshold b value with the ability to separate the active groups from inactive groups was defined as the optimal threshold b value. Three threshold b values encompassing 10, 20, and 30 s/mm^2 were tested. If threshold b value was chosen to be 10 s/mm^2, then b values of 10, 20, 30, 50, 600, and 800 s/mm^2 were used to measure D_{slow}. With threshold b value of 30 s/mm^2, then, D_{slow} was obtained using b values including 30, 50, 600, and 800 s/mm^2.

2.4. Statistical Analysis. Statistical analysis was performed with Statistical Product and Service Solutions (SPSS) version 22.0 (IBM, Armonk, NY). All measurements were expressed as the mean ± standard deviation (SD) and were illustrated with Bland–Altman plot. The examinee and patient were grouped as follows: active group ($n = 40$) vs. the inactive group ($n = 144$), active group vs. the control group ($n = 20$), and inactive group vs. the control group. The Kruskal-Wallis test was used to test the difference among the three groups. The parameters (D_{slow}, f, and D_{fast}) between every two groups were separately tested by the one-way ANOVA test. Receiver operating characteristic (ROC) curve analysis was used to evaluate the diagnostic performance of D_{slow}, f , and D_{fast} between two groups. Diagnostic performance of area under the curve (AUC) values was defined as follows: <0.7, low; 0.7–0.9, medium; and >0.9, high, respectively. $P < 0.017$ was considered statistically significant.

3. Results

3.1. Patient and Lesion Characteristics. According to our inclusion and exclusion criteria, a total of 184 patients (137 males, 47 females; mean age, 28.62 ± 9.26 years; age range, 12–64 years) with axSpA were eventually enrolled in this study, including 40 patients (28%) in the active group and 144 patients (72%) in inactive groups. Patient characteristics are shown in Table 2. No statistical differences were identified between the active and inactive groups for age, gender, disease duration, and BASDAI score (all $P < 0.05$), while both ESR and CRP had a significant difference between the two groups. For BME lesions, hypointense or isointense lesions were observed in sacral and iliac bones of the sacroiliac joint on TSE T1W images and f maps, and hyperintense lesions in affected areas were shown on axial T2W and SPAIR T2W images and Dsmaps. 34 patients (85%) with BME and 6 patients (15%) with non-BME were in the active group, while 117 patients (81.51%) with non-BME and 27 patients (18.49%) with BME were in the inactive group.

3.2. Comparison of Parameters Derived from IVIM DWI in the Three Groups with Different Threshold b Values. Excellent intra- and interobserver agreement of D_{slow}, f, and D_{fast} could be found in Table 3. For any threshold b value studied for the intraobserver correlation coefficient, the lowest mean values of D_{slow}, f, and D_{fast} are 0.895, 0.832, and 0.873, respectively. For any threshold b value studied for the interobserver correlation coefficient, the lowest values of D_{slow}, f, and D_{fast} are 0.993, 0.848 and 0.859, respectively.

As shown in Figure 1(b), the signal intensity of all b values fitted well to the biexponential model with a $R^2 = 1\text{-SSE/SS}_{total}$. (Figure 1(b)). The comparison of D_{slow}, D_{fast}, and f of the three groups is described in Table 4 and Figure 2 with different threshold b values. We found significant differences among the three groups for D_{slow} and D_{fast} adopting threshold b values of 10, 20, or 30 s/mm^2 (all $P < 0.001$). Moreover, D_{slow} and D_{fast} were statistically different between any two groups (all $P < 0.05$). In terms of f, significant differences were observed in the active group vs. the inactive group and the active group vs. control group utilizing optimal threshold b value of 30 s/mm^2 (both $P < 0.05$), while there was no difference between every two remaining

Table 2: Summary of axSpA patients' characteristics.

Parameter	Active group	Inactive group	P value
Age (y)	29.95 ± 9.92	28.25 ± 9.03	0.31
Gender (male/female)*	31/9	106/38	0.62
Disease duration (m)	54.90 ± 62.42	45.37 ± 46.69	0.37
ESR (mm/h)	29.24 ± 24.58	10.27 ± 9.81	<0.001
CRP (mg/dL)	24.27 ± 40.18	6.48 ± 12.59	0.01
BASDAI score	3.47 ± 2.26	2.53 ± 1.72	0.08

Except where indicated, data are the means ± standard deviations. AxSpA: axial spondyloarthritis; BME: bone marrow edema; ESR: erythrocyte sedimentation rate; CRP: C-reactive protein; BASDAI: bath ankylosing spondylitis disease activity index. *Data are numbers of participants.

Table 3: Intra- and interobserver agreement in the assessment of D_{slow}, f, and D_{fast}.

Parameters	Intra- and interclass coefficient correlation (95% CI)	
	Intraobserver	Interobserver
Threshold $b = 10$ s/mm^2		
D_{slow} ($\times 10^{-3}$ mm^2/s)	0.992 (0.985-0.996)	0.993 (0.987-0.997)
f (%)	0.859 (0.750-0.923)	0.954 (0.915-0.975)
D_{fast} ($\times 10^{-3}$ mm^2/s)	0.873 (0.775-0.931)	0.914 (0.841-0.954)
Threshold $b = 20$ s/mm^2		
D_{slow} ($\times 10^{-3}$ mm^2/s)	0.990 (0.980-0.995)	0.994 (0.988-0.997)
f (%)	0.923 (0.859-0.958)	0.848 (0.721-0.919)
D_{fast} ($\times 10^{-3}$ mm^2/s)	0.894 (0.809-0.942)	0.949 (0.907-0.973)
Threshold $b = 30$ s/mm^2		
D_{slow} ($\times 10^{-3}$ mm^2/s)	0.895 (0.811-0.943)	0.995 (0.991-0.997)
f (%)	0.832 (0.705-0.907)	0.899 (0.818-0.945)
D_{fast} ($\times 10^{-3}$ mm^2/s)	0.897 (0.814-0.944)	0.898 (0.816-0.945)

D_{slow}: pure diffusion coefficient; f: perfusion fraction; D_{fast}: pseudoperfusion coefficient; CI: confidence interval.

Table 4: Comparison of D_{slow}, f, and D_{fast} of patients in the active, inactive, and control groups using different threshold b values.

Parameter	Active group	Inactive group	Control group	P
Threshold $b = 10$ s/mm^2				
D_{slow} (10^{-3} mm^2/s)	0.953 ± 0.300	0.405 ± 0.171$^{\#}$	0.286 ± 0.080$^{\#,*}$	<0.001
f (%)	17.953 ± 9.251	15.068 ± 6.674	15.091 ± 8.396	0.751
D_{fast} (10^{-3} mm^2/s)	108.971 ± 45.037	153.790 ± 42.069$^{\#}$	182.938 ± 37.665$^{\#,*}$	<0.001
Threshold $b = 20$ s/mm^2				
D_{slow} (10^{-3} mm^2/s)	0.980 ± 0.284	0.414 ± 0.174$^{\#}$	0.293 ± 0.085$^{\#,*}$	<0.001
f (%)	24.105 ± 8.481	20.416 ± 7.033	19.673 ± 9.562	0.172
D_{fast} (10^{-3} mm^2/s)	110.590 ± 35.003	141.334 ± 34.207$^{\#}$	159.995 ± 45.047$^{\#,*}$	<0.001
Threshold $b = 30$ s/mm^2				
D_{slow} (10^{-3} mm^2/s)	0.973 ± 0.286	0.408 ± 0.171$^{\#}$	0.283 ± 0.069$^{\#,*}$	<0.001
f (%)	19.985 ± 5.757	16.934 ± 7.437	13.293 ± 9.853$^{\#}$	0.031
D_{fast} (10^{-3} mm^2/s)	79.748 ± 28.815	98.595 ± 26.569$^{\#}$	116.155 ± 36.301$^{\#,*}$	<0.001

Except where indicated, data are the means ± standard deviations. D_{slow}: pure diffusion coefficient; f: perfusion fraction; D_{fast}: pseudoperfusion coefficient. $^{\#}P < 0.05$ vs. the active group; $^{*}P < 0.05$ vs. the inactive group. $P < 0.017$ was considered statistically significant.

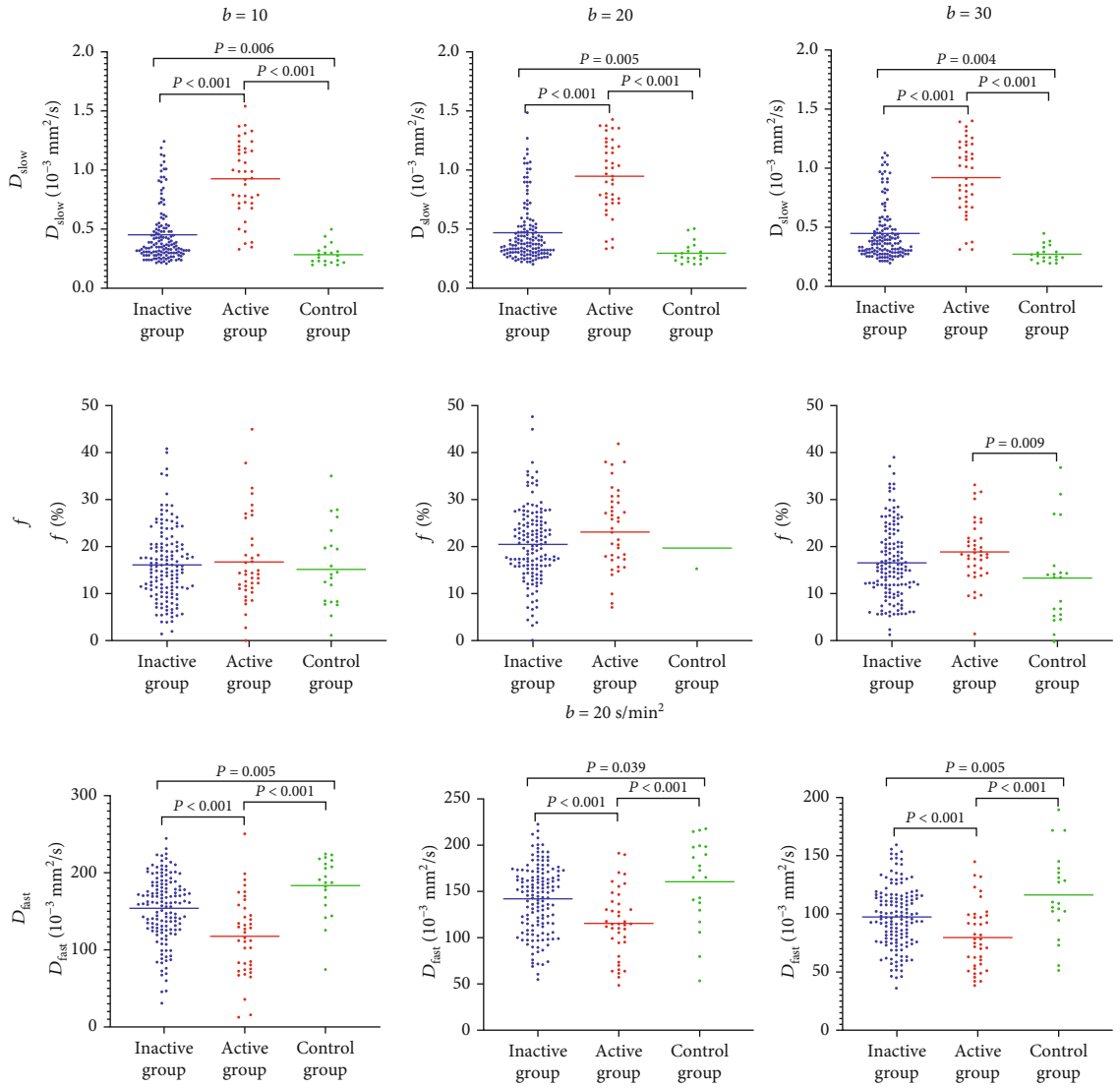

Figure 2: Scattered plots for D_{slow}, f, and D_{fast} in the active, inactive, and control groups. All data were analyzed by analysis of variance and tested by one-way ANOVA test with P value < 0.05 as a statistically significant difference.

Table 5: ROC curve analysis for D_{slow}, f, and D_{fast} in the active, inactive, and control groups.

Parameter	Active group-inactive group AUC [cutoff value] (sensitivity, specificity, accuracy)	Active group-control group AUC [cutoff value] (sensitivity, specificity, accuracy)	Inactive group-control group AUC [cutoff value] (sensitivity, specificity, accuracy)
Threshold $b = 10$ s/mm^2			
D_{slow} (10^{-3} mm^2/s)	0.877 [0.654] (0.825, 0.840, 0.837)	0.981 [0.501] (0.875, >0.999, 0.900)	0.778 [0.307] (0.701, 0.750, 0.707)
f (%)	0.499 [-] (-)	0.551 [8.510] (0.875, 0.350, 0.700)	0.548 [8.614] (0.840, 0.350, 0.780)
D_{fast} (10^{-3} mm^2/s)	0.283 [-] (-)	0.145 [-] (-)	0.283 [-] (-)
Threshold $b = 20$ s/mm^2			
D_{slow} (10^{-3} mm^2/s)	0.882 [0.578] (0.900, 0.806, 0.821)	0.981 [0.538] (0.900, >0.999, 0.933)	0.776 [0.298] (0.757, 0.700, 0.756)
f (%)	0.595 [25.343] (0.475, 0.757, 0.696)	0.632 [25.164] (0.475, 0.850, 0.600)	0.565 [13.669] (0.833, 0.350, 0.774)
D_{fast} (10^{-3} mm^2/s)	0.306 [-] (-)	0.214 [-] (-)	0.352 [-] (-)
Threshold $b = 30$ s/mm^2			
D_{slow} (10^{-3} mm^2/s)	0.881 [0.605] (0.875, 0.833, 0.842)	0.980 [0.519] (0.900, >0.999, 0.933)	0.794 [0.304] (0.722, 0.750, 0.720)
f (%)	0.613 [13.743] (0.875, 0.410, 0.512)	0.738 [14.486] (0.800, 0.750, 0.783)	0.644 [14.474] (0.576, 0.750, 0.598)
D_{fast} (10^{-3} mm^2/s)	0.316 [-] (-)	0.205 [-] (-)	0.346 [-] (-)

Data are areas under the curve. Numbers in parentheses are cutoff values. AUC: area under the curve; ROC: receiver operating characteristic; D_{slow}: pure diffusion coefficient; f: perfusion fraction; D_{fast}: pseudoperfusion coefficient.

groups with threshold b values of 10, 20, and 30 s/mm^2 (all $P \geq 0.05$).

3.3. ROC Curve Analysis for Parameters Derived from IVIM DWI for the Detection of the Activity in axSpA Patients. Table 5 and Figure 3 show the three-group ROC analysis of IVIM parameters using threshold b values of 10, 20, and 30 s/mm^2. D_{slow} demonstrated the most perfect differentiation between the active and the control groups with high AUC values with threshold b values of 10, 20, and 30 s/mm^2 (0.981, 0.981, and 0.980, respectively). And it achieved accuracy of 0.900, 0.933, and 0.933 with sensitivity of 0.875, 0.900, and 0.900 and specificity of 1.000, 1.000, and 1.000, respectively. Also, it provided moderate performance to discriminate active groups from inactive groups and inactive groups from control groups with medium AUC values with threshold b values of 10, 20, and 30 s/mm^2. f only showed the moderate performance to separate the active group from the control groups with the medium AUC value of 0.738 and the cutoff value of 14.486% utilizing the optimal threshold b value of 30 s/mm^2. With the increasing of the threshold b value (from 10 to 30 s/mm^2), the AUC among three groups also increased. D_{fast} presented low performance (all AUC < 0.35) with threshold b values of 10 and 30.

4. Discussion

Our study investigated the performance of D_{slow}, f, and D_{fast} to detect the activity in patients with axSpA using IVIM DWI with threshold b values of 10, 20, and 30 s/mm^2. We confirmed that the optimal threshold b value was 30 s/mm^2. Using the optimal threshold b value of 30 s/mm^2, D_{slow} provided the best performance to detect the activity in axSpA patients, and f showed the moderate performance to discriminate the axSpA patients in the active stage from those in the inactive stage, while the disease activity could not be diagnosed by D_{fast} in axSpA patients.

In our study, a large sample size of 184 patients was analyzed, and thus, the results based on the optimal threshold b values were more persuasive for the detection of the axSpA activity in sacroiliitis. Previous studies confirmed that, with a carefully selected threshold b value, the error could be reduced in the measurement of parameters from IVIM DWI [22, 23]. However, it is demonstrated that the optimal threshold b value is dependent on the location of the body, such as 40 s/mm^2 in breast cancer and 100 s/mm^2 in cervical adenocarcinoma [24, 25]. In this study, we found the optimal threshold for sacroiliitis was 30 s/mm^2 in axSpA patients, which has not seen reported. Compared with the threshold b values of 10 and 20 s/mm^2, a b value of 30 s/mm^2 increases the AUC (cutoff value) for perfusion parameters (f and D_{fast}) between the active and the inactive groups (the result is provided in Table 5 and also shown in Figure 3). Previous studies showed that f and D_{fast} had no statistical differences between the active and inactive groups in axSpA patients, so perfusion parameters derived from IVIM DWI could not be used to distinguish the active from the inactive axSpA patients [10]. However, our

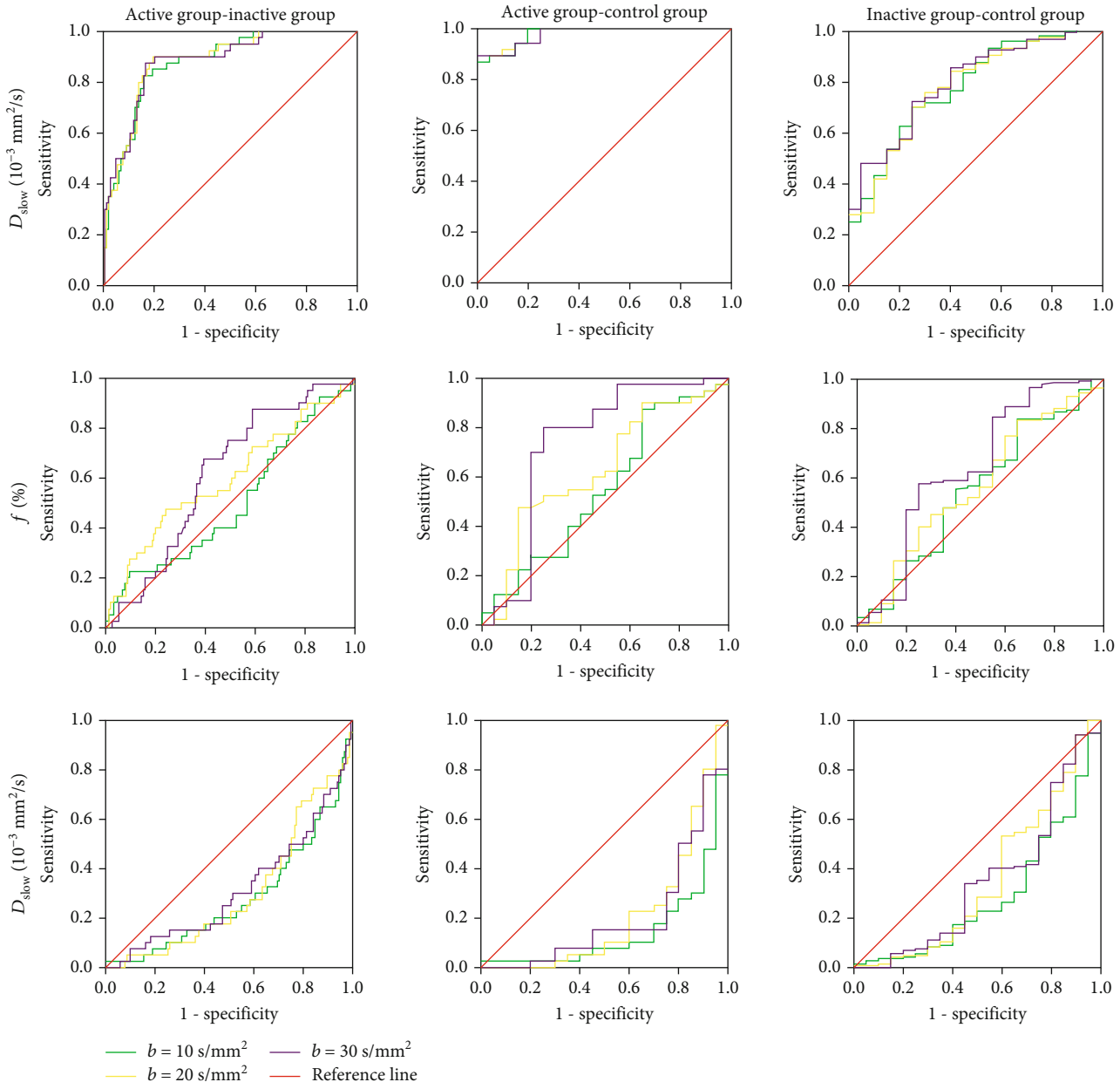

FIGURE 3: The receiver operating characteristic (ROC) curve for D_{slow}, f, and D_{fast} in the active, inactive, and control groups (threshold b value: 30 s/mm^2).

results confirmed that the activity could be detected by f in axSpA patients and the AUC for f was 0.613 (13.743) between the active and the inactive groups with the threshold b values of 30 s/mm^2. This improvement was expected to be potential clinical values for detecting the activity of the axSpA patients.

Furthermore, which is due to the different effect on D_{slow} from the threshold b values of 10, 20, and 30 s/mm^2. Therefore, the results for D_{slow} presented in Figure 2 should be identical. The authors should explain why there are differences. b value = 200 s/mm^2 has been popularly used to detect the disease activity of axSpA patients for the IVIM DWI threshold [8, 12]. When using a threshold b value of 200 s/mm^2, the contributions of the perfusion or diffusion to D_{slow} or f/D_{fast} are considered to be neglect. In our study, the results of D_{slow} presented differences in the same way for the three different cases; however, there is no statistical difference between them. We considered that the threshold b values of 10, 20, and 30 s/mm^2 effected on diffusion to D_{slow}. Recently, several studies suggested that this threshold b value may be too high as the turning point of a biexponential model is generally around 50 s/mm^2 [15]. Our results also suggested a b value of 30 s/mm^2 should be selected for separating active patients with axSpA from inactive ones, which also corresponds to the turning point of the biexponential model for the IVIM DWI fitting curve.

So far as we know, it remains unclear whether f can identify the axSpA activity using the full IVIM model [12]. In this study, we disclosed that f may have the ability to detect the axSpA activity with the optimal threshold b value of 30 s/mm^2. Active sacroiliitis increases the ratio of extracellular water to intracellular water and the movement of water molecules, which is also associated with increased microvascular perfusion[26]. In previous studies, D_{slow} has been confirmed to be the most reliable parameter among the three parameters (D_{slow}, f, and D_{fast}) for detecting the activity of sacroiliitis in axSpA patients [8, 10, 11, 27]. Although the b value of 0 s/mm^2 was excluded in our measurements, D_{slow} with threshold b values of 10, 20, and 30 s/mm^2 was still the most effective indicator of disease activity. f and D_{fast} in the IVIM model is related to perfusion [28]. The optimal threshold b value dramatically improved the diagnostic performance for f. D_{fast} demonstrated the poor diagnostic performance despite using any threshold b value, in agreement with the result reported for the full IVIM model by Li et al. [15]. This result can be explained that D_{fast} tends to be unstable unless an unrealistically high signal-to-noise ratio (SNR) is achieved to an SNR of >122.48, while f can reach to be steady at a moderate SNR of 40.48 [29]. Thereby, a combination of D_{slow} and f with the optimal threshold value of 30 s/mm^2 could supply more accurate information to detect the axSpA activity.

Several limitations remained in current our study. Firstly, taking scanning times for patients into account, the relatively fewer numbers of 7 b values were utilized to probe threshold b values in this study, which might reduce the accuracy of the parameters from IVIM DWI. Generally, the optimal b value distribution could dramatically amplify IVIM parameter reliability, and the number of threshold b values ranging from 6 to 12 is even suggested to be the minimal applied number in liver disease detection [30, 31]. Second, the relationship between bone mineral density (BMD) and IVIM parameters is not covered in our study. Some studies believe that IVIM parameters are affected by BMD[32, 33]. Hence, an investigation of the influence of BMD on IVIM DWI is desirable in sacroiliitis in the future. Thirdly, b values that be selected and evaluated for the biexponential algorithm in this study are quite arbitrary and empirical, which violates the free distribution of parameters. In future studies, more b values will be studied and evaluated.

In conclusion, this study confirmed that D_{slow} has been confirmed to be the most reliable parameter among the three parameters (D_{slow}, f, and D_{fast}) for detecting the activity of sacroiliitis in axSpA patients. f will promisingly increase the diagnostic accuracy of the axSpA activity to improve treatment for patients with axSpA using the optimal threshold b value of 30 s/mm^2, whereas D_{fast} will not.

Abbreviations

IVIM: Intravoxel incoherent motion
DWI: Diffusion-weighted imaging
axSpA: Axial spondyloarthritis
AUC: Area under the curve
SIJ: Sacroiliac joints
MRI: Magnetic resonance imaging
AxSpA: Axial spondyloarthritis
SNR: Signal-to-noise ratio
IRB: Institutional review board
ESR: Erythrocyte sedimentation rate
CRP: C-reactive protein
ASDAS: Spondyloarthritis disease activity score
ROI: Region of interest
ICC: Intraclass correlation coefficient
BME: Bone marrow edema
SSE: Sum of squares due to error
SPSS: Statistical product and service solutions
IBM: International business machines
SD: Standard deviation
ROC: Receiver operating characteristic
BMD: Bone mineral density.

Data Availability

All the data related to this study are mentioned in the manuscript. Any further data if required may be obtained on request from the corresponding author.

Conflicts of Interest

The authors declare no conflicts of interest.

Authors' Contributions

Qiang Ye and Zhuoyao Xie contributed equally to this work.

Acknowledgments

This paper is supported by the National Natural Science Foundation of China (Grant No. 81871510).

References

[1] W. Zhu, X. He, K. Cheng et al., "Ankylosing spondylitis: etiology, pathogenesis, and treatments," *Bone Research*, vol. 7, no. 1, 2019.

[2] J. Braun and T. Pincus, "Mortality, course of disease and prognosis of patients with ankylosing spondylitis," *Clinical and Experimental Rheumatology*, vol. 20, 6, Supplement 28, pp. S16–S22, 2002.

[3] J. Braun and J. Sieper, "Ankylosing spondylitis," *The Lancet*, vol. 369, no. 9570, pp. 1379–1390, 2007.

[4] P. C. Robinson, R. Sengupta, and S. Siebert, "Non-radiographic axial spondyloarthritis (nr-axSpA): advances in Classification, Imaging and Therapy," *Imaging and Therapy. Rheumatology and Therapy*, vol. 6, no. 2, pp. 165–177, 2019.

[5] C. Tsoi, J. F. Griffith, R. K. L. Lee, P. C. H. Wong, and L. S. Tam, "Imaging of sacroiliitis: current status, limitations and pitfalls," *Quantitative Imaging in Medicine and Surgery*, vol. 9, no. 2, pp. 318–335, 2019.

[6] V. Strand and J. A. Singh, "Evaluation and management of the patient with suspected inflammatory spine disease," *Mayo Clinic Proceedings*, vol. 92, no. 4, pp. 555–564, 2017.

[7] D. Le Bihan, E. Breton, D. Lallemand, P. Grenier, E. Cabanis, and M. Laval-Jeantet, "MR imaging of intravoxel incoherent

motions: application to diffusion and perfusion in neurologic disorders," *Radiology*, vol. 161, no. 2, pp. 401–407, 1986.

[8] J. Qin, J. Li, H. Yang et al., "Values of intravoxel incoherent motion diffusion weighted imaging and dynamic contrast-enhanced MRI in evaluating the activity of sacroiliitis in ankylosing spondylitis of rat model," *Magnetic Resonance Imaging*, vol. 68, pp. 30–35, 2020.

[9] L. A. Bradbury, K. A. Hollis, B. Gautier et al., "Diffusion-weighted imaging is a sensitive and specific magnetic resonance sequence in the diagnosis of ankylosing spondylitis," *The Journal of Rheumatology*, vol. 45, no. 6, pp. 771–778, 2018.

[10] Y. H. Zhao, S. L. Li, Z. Y. Liu et al., "Detection of active sacroiliitis with ankylosing spondylitis through intravoxel incoherent motion diffusion-weighted MR imaging," *European Radiology*, vol. 25, no. 9, pp. 2754–2763, 2015.

[11] Y. Zhao, Q. Zhang, W. Li et al., "Assessment of correlation between intravoxel incoherent motion diffusion weighted MR imaging and dynamic contrast-enhanced MR imaging of sacroiliitis with ankylosing spondylitis," *BioMed Research International*, vol. 2017, Article ID 8135863, 9 pages, 2017.

[12] H. Sun, K. Liu, H. Liu et al., "Comparison of bi-exponential and mono-exponential models of diffusion-weighted imaging for detecting active sacroiliitis in ankylosing spondylitis," *Acta Radiologica*, vol. 59, no. 4, pp. 468–477, 2018.

[13] H. A. Dyvorne, N. Galea, T. Nevers et al., "Diffusion-weighted imaging of the liver with MultiplebValues: effect of diffusion gradient polarity and breathing acquisition on image quality and intravoxel incoherent motion Parameters—A pilot study," *Radiology*, vol. 266, no. 3, pp. 920–929, 2013.

[14] C. Vieni, B. Ades-Aron, B. Conti et al., "Effect of intravoxel incoherent motion on diffusion parameters in normal brain," *Neuro Image*, vol. 204, p. 116228, 2020.

[15] Y. T. Li, J. P. Cercueil, J. Yuan, W. Chen, R. Loffroy, and Y. X. Wáng, "Liver intravoxel incoherent motion (IVIM) magnetic resonance imaging: a comprehensive review of published data on normal values and applications for fibrosis and tumor evaluation," *Quantitative Imaging in Medicine and Surgery*, vol. 7, no. 1, pp. 59–78, 2017.

[16] Y. X. J. Wáng, Y. T. Li, O. Chevallier et al., "Dependence of intravoxel incoherent motion diffusion MR thresholdb-value selection for separating perfusion and diffusion compartments and liver fibrosis diagnostic performance," *Acta radiologica*, vol. 60, no. 1, pp. 3–12, 2019.

[17] M. Rudwaleit, D. van der Heijde, R. Landewe et al., "The development of assessment of SpondyloArthritis international society classification criteria for axial spondyloarthritis (part II): validation and final selection," *Annals of the Rheumatic Diseases*, vol. 68, no. 6, pp. 777–783, 2009.

[18] J. Sieper, M. Rudwaleit, X. Baraliakos et al., "The Assessment of SpondyloArthritis international Society (ASAS) handbook: a guide to assess spondyloarthritis," *Annals of the rheumatic diseases*, vol. 68, Suppl 2, pp. ii1–ii44, 2009.

[19] M. N. Magrey and U. Kiltz, "Chapter 9- clinical assessment of axial Spondyloarthritis," in *Khan MA, Editors*, P. Mease, Ed., pp. 121–133, Elsevier, Axial Spondyloarthritis, 2019.

[20] D. Le Bihan, R. Turner, and J. R. Macfall, "Effects of intravoxel incoherent motions (IVIM) in steady-state free precession (SSFP) imaging: application to molecular diffusion imaging," *Magnetic Resonance in Medicine*, vol. 10, no. 3, pp. 324–337, 1989.

[21] D. Le Bihan, E. Breton, D. Lallemand, M. L. Aubin, J. Vignaud, and M. Laval-Jeantet, "Separation of diffusion and perfusion in intravoxel incoherent motion MR imaging," *Radiology*, vol. 168, no. 2, pp. 497–505, 1988.

[22] J. A. U. Perucho, H. C. C. Chang, V. Vardhanabhuti et al., "B-value optimization in the estimation of intravoxel incoherent motion parameters in patients with cervical cancer," *Korean Journal of Radiology*, vol. 21, no. 2, pp. 218–227, 2020.

[23] O. Jalnefjord, M. Montelius, G. Starck, and M. Ljungberg, "Optimization of b-value schemes for estimation of the diffusion coefficient and the perfusion fraction with segmented intravoxel incoherent motion model fitting," *Magnetic Resonance in Medicine*, vol. 82, no. 4, pp. 1541–1552, 2019.

[24] A. S. Becker, J. A. Perucho, M. C. Wurnig et al., "Assessment of cervical cancer with a parameter-free intravoxel incoherent motion imaging algorithm," *Korean Journal of Radiology*, vol. 18, no. 3, pp. 510–518, 2017.

[25] W. Chen, J. Zhang, D. Long, Z. Wang, and J. M. Zhu, "Optimization of intra-voxel incoherent motion measurement in diffusion-weighted imaging of breast cancer," *Journal of Applied Clinical Medical Physics*, vol. 18, no. 3, pp. 191–199, 2017.

[26] M. Zhang, L. Zhou, N. Huang, H. Zeng, S. Liu, and L. Liu, "Assessment of active and inactive sacroiliitis in patients with ankylosing spondylitis using quantitative dynamic contrast-enhanced MRI," *Journal of magnetic resonance imaging: JMRI*, vol. 46, no. 1, pp. 71–78, 2017.

[27] H. T. Sanal, S. Yilmaz, I. Simsek et al., "Apparent diffusion coefficients of sacroiliitis in patients with established ankylosing spondylitis," *Clinical Imaging*, vol. 37, no. 4, pp. 734–739, 2013.

[28] F. Wang, Y. Wang, Y. Zhou et al., "Comparison between types I and II epithelial ovarian cancer using histogram analysis of monoexponential, biexponential, and stretched-exponential diffusion models," *Journal of magnetic resonance imaging: JMRI*, vol. 46, no. 6, pp. 1797–1809, 2017.

[29] J. Pekar, C. T. Moonen, and P. C. van Zijl, "On the precision of diffusion/perfusion imaging by gradient sensitization," *Magnetic Resonance in Medicine*, vol. 23, no. 1, pp. 122–129, 1992.

[30] M. C. Wurnig, O. F. Donati, E. Ulbrich et al., "Systematic analysis of the intravoxel incoherent motion threshold separating perfusion and diffusion effects: proposal of a standardized algorithm," *Magnetic resonance in medicine*, vol. 74, no. 5, pp. 1414–1422, 2015.

[31] E. E. ter Voert, G. Delso, M. Porto et al., "Intravoxel incoherent motion protocol evaluation and data quality in normal and malignant liver tissue and comparison to the literature," *Investigative Radiology*, vol. 51, no. 2, pp. 90–99, 2016.

[32] D. Yeung, S. Wong, J. F. Griffith, and E. Lau, "Bone marrow diffusion in osteoporosis: evaluation with quantitative MR diffusion imaging," *Journal of Magnetic Resonance Imaging*, vol. 19, no. 2, pp. 222–228, 2004.

[33] N. Ohno, T. Miyati, H. Kasai et al., "Evaluation of perfusion-related and true diffusion in vertebral bone marrow: a preliminary study," *Radiological Physics and Technology*, vol. 8, no. 1, pp. 135–140, 2014.